Performance of the GSN station KONO-IU, 1991-2009

A report in a series documenting the status of the Global Seismographic Network

WQC Report 2010:9
February 28, 2010

Göran Ekström and Meredith Nettles

Waveform Quality Center
Lamont-Doherty Earth Observatory of Columbia University, New York

1 Station performance report: KONO

This report summarizes a number of observations that are relevant for assessing the past and current quality of the data recorded at one of the stations of the Global Seismographic Network. The purpose of the report is, in part, to document specific problems observed with the data. Some of these problems are related to errors in the available descriptions of station parameters: orientation of the sensors, response functions, polarities. In principle, such errors in the station metadata can be corrected by providing updated station parameters. In practice, this may be difficult in some cases due to lack of knowledge of, or inability to determine, the correct parameters. Other problems are caused by the malfunctioning of some instrument component. Regardless of the cause, it is necessary to document and publicize the lack of accurate and reliable station characteristics, especially when it is not obvious from simple inspection of the data that a problem exists. It is also of value to document the characteristics of stations performing well, both to establish their high quality and to help identify installation and operation procedures that should be emulated at other stations.

1.1 Station KONO

The station KONO (Kongsberg) is located in a historic silver mine near the city of Kongsberg in southern Norway (see Figure 1). It is in a very good location for providing global coverage in earthquake and Earth structure studies. The closest GSN station is ESK-II (Eskdalemuir) in Scotland, approximately 900 km southwest of KONO.

KONO is part of the USGS (IU) component of the IRIS/USGS Global Seismographic Network.

1.2 The data

Digital broadband seismic data from KONO are available from the IRIS DMC beginning in 1991. Prior to becoming a station of the GSN, KONO was an Abbreviated Seismic Research Observatory (ASRO, network code AS) station of the Global Digital Seismic Network (GDSN) (1978–1991) and, as KON, a station of the High Gain Long Period (HGLP, network code HG) network (1972–1978). Here, we consider broadband GSN instruments at the station beginning in 1991. The initial GSN installation consisted of a set of STS-1 seismometers. An auxiliary STS-2 sensor was installed in 1999. Data from KONO are included

in our standard CMT analysis (Dziewonski et al., 1981; Ekström et al., 2005), and waveform data, travel-time observations, and dispersion curves derived from KONO data have been used in the development of numerous global and regional tomographic models since the station was installed.

In the analyses described here, we have made use of data collected from the IRIS DMC. We requested and downloaded all long-period (LH) and very-long-period (VH) data available at the DMC for both sensors from the start of operation (1991) until September 2009. We used the currently available station metadata prepared by the Albuquerque Seismological Laboratory and available at the IRIS DMC (downloaded in December 2009). Overall, the station has been operated with few data outages since 1991.

1.3 The metadata

The dataless SEED volume for KONO documents 6 response epochs for the STS-1 (primary) and STS-2 (secondary) sensors at KONO. The STS-1 1 sps channels were initially called LHZ, LHN, LHE, without a location code. They were renamed with the location code 00 on 1999.040 (040 representing the day of year). We refer to these channels as LHZ-00, LHN-00, and LHE-00. The STS-2 sensor (location code 10) was installed on 1999.040 and we refer to the 1 sps channels as LHZ-10, LHN-10, and LHE-10. The horizontal components were renamed on 2009.255; current 1 sps channel names are LHZ-00, LH1-00, LH2-00, LHZ-10, LH1-10, and LH2-10. Epoch boundaries are given at 1991.171 (first data), 1997.260, 1998.066, 1999.040 (first STS-2 data), 2006.319, 2009.255 (new channel names). The metadata indicate gain changes at some epoch boundaries; no variations in the frequency response are indicated.

1.4 Scaling analysis

One method for assessing the quality of the data is the systematic comparison of recorded long-period waveforms with synthetic seismograms calculated for known seismic events. This analysis follows the steps described by Ekström et al. (2006). Seismic data for the LH and VH channels from both the STS-1 and STS-2 sensors are collected. Corresponding synthetic waveforms for all earthquakes in the Global CMT catalog (Dziewonski et al., 1981; Ekström et al., 2005) with $M_W \geq 6.5$ are calculated. Correlation coefficients and optimal scaling factors between observed and synthetic waveforms are calculated for the three types of data used in the standard CMT analysis: body waves (B), with periods in the range 50–150 sec, mantle waves (M), with periods in the range 125–350 sec, and surface waves (S), with periods in the range 50–150 sec. Body- and mantle-wave results are discussed here. The scaling factor is only calculated for waveforms with a correlation of 0.75 or greater. The scaling factor is the number by which the synthetic seismogram should be multiplied to maximize the agreement with the observed seismogram. Annual median values of the scaling factors are calculated when four or more individual event scaling estimates are available for the year. Reversed components can be identified by their large negative correlations.

Figure 2 shows the results of our systematic comparison of KONO waveforms with synthetic seismograms. From 1991 until the present, the STS-1 signals for large earthquakes correlate well with synthetic waveforms. The STS-2 seismometer, installed in 1999, also generates seismograms that correlate well with to synthetic waveforms. A gap of several months in scaling-factor measurements in late 2004 through early 2005 corresponds to a period with large timing errors in the data.

1.5 Noise analysis

A second method for investigating the overall performance of the sensors is to monitor background noise levels for all seismic channels, after conversion of the data to ground acceleration. We calculate hourly rms values of the time-domain seismic signal in narrow frequency bands, and convert the rms values to a power

spectral density (PSD) at that frequency using Parseval's theorem. For each month, we then calculate the low-noise value at each frequency by determining the PSD amplitude not exceeded 10% of the time.

The PSD data provide much information about the station and the sensors. Figure 3 shows the monthly low-noise estimate for each LH channel at 72-s period since 1991. The first observation is that the station has been providing data without major outages since 1991. Second, the noise data suggest that KONO generally is a quiet site, especially on the STS-1 vertical component. Horizontal STS-1 noise levels were variable between 1997 and 2006, but appear more stable since 2007. Vertical STS-1 noise levels experienced an increase during 2005–2006, but decreased and stabilized in 2007–2009.

Noise levels on the STS-2 sensor have varied with time. During 2004–2006, horizontal noise levels are lower on the STS-2 sensor than on the STS-1 sensor. Since 2007, noise levels on all components of the STS-2 sensor have been high, and the noise on the vertical component increased steadily during 2007–2009.

1.6 Inter-sensor coherence

An additional method for assessing the quality and calibration of the recorded signals is to calculate inter-sensor coherence. This analysis is possible when more than one sensor is operated in the same location. At KONO, this is possible for the period 1999–2009, during which time both STS-1 and STS-2 instruments have operated.

We calculate the coherence of the deconvolved vertical, N–S, and E–W components. The coherence is calculated for $\sim$2-hour-long time windows containing the signals for earthquakes with $M_W \geq 6.5$ (the same events used in the scaling analysis). For each pair of seismograms, the coherence is calculated in narrow frequency bands around 32 s, 64 s, 128 s and 256 s. If the coherence is greater than 0.95, the value is stored together with the complex scaling factor (represented here as a scaling factor and phase shift) that should be applied to the secondary-sensor data to bring the two time series into the best agreement. In the following, the discussion is based on the assumption that the secondary (STS-2) sensor is properly calibrated and that deviations from a scaling factor of 1.0 and a phase shift of 0° should be attributed to differences between the true and reported response functions of the primary (STS-1) sensor.

Figure 4 shows the results of the coherence analysis for the vertical component. The measurements are fairly consistent and stable. The scaling factors at 32 s are close to 1.0 during the entire time period. At longer periods, there is a small deviation consistent with an over-stated gain in the metadata of 5–10% at 256-s period for the STS-1 sensor.

Figure 5 shows the amplitude and phase differences for the N–S components. A relatively large scatter of scaling measurements corresponding to gain variations of $\pm$10% is seen, with a possible reduction in the scatter following the epoch boundary at 2006.319. Scaling factors at 128-s period and 256-s period generally become closer to 1.0 after this boundary.

Figure 6 shows the results for the E–W component, which are similar to those for the N–S component, although the scatter in the measurements is smaller. A clear trend is seen between 2004 and late 2006 reflecting a loss of long-period gain and a corresponding phase shift. This is similar to the gradual loss of long-period gain observed at other GSN stations, e.g., KIP (Ekström and Nettles, WQC Report 2010:2). The long-period gain appears to have recovered after the epoch boundary at 2006.319.

Given that we use the same selection criteria for the coherence for all three components, we do not yet understand the source of the differences in the level of scatter seen for the different components.

1.7 Polarization analysis

The orientation of the horizontal components can be assessed empirically by comparing observed and synthetic waveforms, and finding the angle by which the horizontal components should be rotated in order to maximize the agreement. We follow the approach described by Ekström and Busby (2008) for such a comparison, using the observed and synthetic waveforms from Global CMT analysis.

We apply the method of Ekström and Busby (2008) to the same dataset used in the scaling analysis. Figure 7 shows the individual measurements for the period of operation for the different channels. The time period in 2004–2005 with no measurements corresponds to a period when the timing of the data was incorrect. The median rotation angles for the STS-1 are 2° for the LHN-00, LHE-00 epoch of measurements, and 3° for the LHN, LHE epoch. For the STS-2 the median angle is 3°. The spreads in the measurements are relatively small for both sensors. There are not enough estimates for the most recent epoch to estimate a rotation angle for the LH1, LH2 channels. The median estimates for the entire period of operation are given in Table 1.

Comp. 1	Comp. 2	First	Last	# Obs.	N	Az 1	Az 2	25%	Med.	75%
LHE	LHN	19910623	19990206	325	82	90	0	1	3	7
LHE-00	LHN-00	19990304	20090902	427	84	90	0	-3	2	3
LHE-10	LHN-10	19990304	20090902	427	82	90	0	-2	3	6
LH1-00	LH2-00	20090929	20090930	2	0	1.2	91.2	-	-	-
LH1-10	LH2-10	20090929	20090930	2	0	2.2	92.2	-	-	-

Table 1: Statistics of sensor-rotation angles estimated in this study. Columns are the channel names, the dates of the first and last observations considered in making the estimate, the total number of observations, the number of observations of acceptable quality, the reported azimuths of sensitivity of the two channels, the median polarization-angle deviation from the reported orientation together with the range of the second (25%) and third (75%) quartiles of the observations.

1.8 Example seismograms

The anomalies described here agree with observations we have made in our routine analysis of waveforms for the determination of CMT earthquake parameters. When confronted with the seismograms for an individual earthquake, it is often difficult to assess whether a poor fit is due to incorrect source parameters, inadequate modeling of wave propagation through an Earth model, or some problem with the recorded seismograms. Here, we have included some examples of data that illustrate the characteristics of the types of problems that we have encountered with data from the KONO station.

Figure 8 shows an example of three-component surface-wave data for an earthquake on November 2, 2004. This corresponds to a period during which there is a timing problem with the data. For this earthquake, the timing error appears to be approximately 60 seconds. Apart from the timing problem, the observed waveforms appear to be similar to the synthetic waveforms.

The top panel of Figure 9 shows a comparison between mantle-wave seismograms recorded on the STS-1 seismometer and the corresponding synthetic waveforms for an event on November 15, 2006. The horizontal components are noticeably too small with respect to the synthetic seismograms, resulting in scaling factors of 0.690 and 0.715. The seismograms from the STS-2 are better fit by the synthetic waveforms, and have corresponding scaling factors of 0.824 and 0.909. This is consistent with the coherence analysis (Figure 5 and Figure 6), which suggests that the E–W STS-1 suffered a loss of long-period gain during 2006, and that the reported N–S STS-1 gain is too large at longer periods prior to 2007.

Figure 10 shows a comparison of mantle-wave seismograms from the STS-1 and STS-2 sensors and corresponding synthetic waveforms for an earthquake on September 30, 2009. This corresponds to the current response epoch. The scaling factors for the two sensors are similar, consistent with the results from the coherence analysis (Figure 5 and Figure 6). Large noise pulses are seen on the LH1 (formerly LHN) channel of the STS-1 sensor; the spikes do not appear on the STS-2.

2 Summary and analysis

At the time of writing (February, 2010), the GSN station KONO is performing relatively well. Our analysis suggests that the station has produced GSN-quality data for much of the period since 1991, although there are periods of several months with erroneous timing of the data (also reported in station Data Problem Reports), and anomalous long-period response. The STS-2 has most of the time provided useful backup data streams, but noise levels on this sensor have been unstable, especially since 2007.

The coherence analysis for the vertical component indicates that the STS-1 long-period gain may be overstated in the metadata, such that the reported shape of the frequency response is not correct. The analysis suggests a gain error of 5–10% at 256 s. The coherence analysis for the horizontal components shows a deterioration of the STS-1 long-period gain, especially on the E–W component, during 2005–2006 before the 2006.319 epoch boundary. This trend is similar to the deterioration seen at several other stations equipped with STS-1 seismometers (Ekström et al., 2006).

A large scatter is seen in the horizontal coherence measurements. We do not have an explanation for this scatter at the current time.

Our scaling and polarization analysis failed for those periods when the timing errors at KONO were of sufficient magnitude that observed and synthetic waveforms no longer correlated. We estimate that with our current tools, we are able to identify timing errors larger than $\sim$20 s.

3 Conclusions and recommendations

This analysis shows that KONO currently is generating data of high quality. While more detailed analysis would be required to establish that the response characteristics are accurate to within the 1% tolerance of the GSN design goals (IRIS, 1985; Lay et al., 2002), our assessment is that, at least at long periods, KONO typically generates data that is close to GSN quality. However, the station history is mixed, and it would be desirable to understand what has caused the variations in the noise levels and inter-sensor coherence over time.

4 References

Dziewonski, A. M., T.-A. Chou, and J. H. Woodhouse, Determination of earthquake source parameters from waveform data for studies of global and regional seismicity, *J. Geophys. Res.*, 86, 2825–2853, 1981.

Ekström, G., A. M. Dziewonski, N. N. Maternovskaya, and M. Nettles, Global seismicity of 2003: Centroid-moment tensor solutions for 1087 earthquakes, *Phys. Earth Planet. Inter.*, 148, 327–351, 2005.

Ekström, G., C. A. Dalton, and M. Nettles, Observations of time-dependent errors in long-period gain at global seismic stations, *Seism. Res. Lett.*, 77, 12–22, 2006.

Ekström, G., and R. W. Busby, Measurements of seismometer orientation at USArray Transportable and Backbone stations, *Seism. Res. Lett.*, 79, 554-561, 2008.

Ekström, G., and M. Nettles, Performance of the GSN station KIP-IU, 1988–2009, Waveform Quality Center Report 2010:2, 2010.

IRIS, *The design goals for a new global seismographic network*, IRIS GSN committee report, 31 pages, 1985.

Lay, T., J. Berger, R. Buland, R. Butler, G. Ekström, B. Hutt, B. Romanowicz, *Global seismic network design goals update 2002*, IRIS GSN committee report, 2002.

Nettles, M., and G. Ekström, Glacial earthquakes in Greenland and Antarctica, *Annual Reviews*, in review, 2010.

Peterson, J., Observations and modeling of background seismic noise, *U. S. Geol. Surv. Open-file Rep. 93-322*, 1–45, 1993.

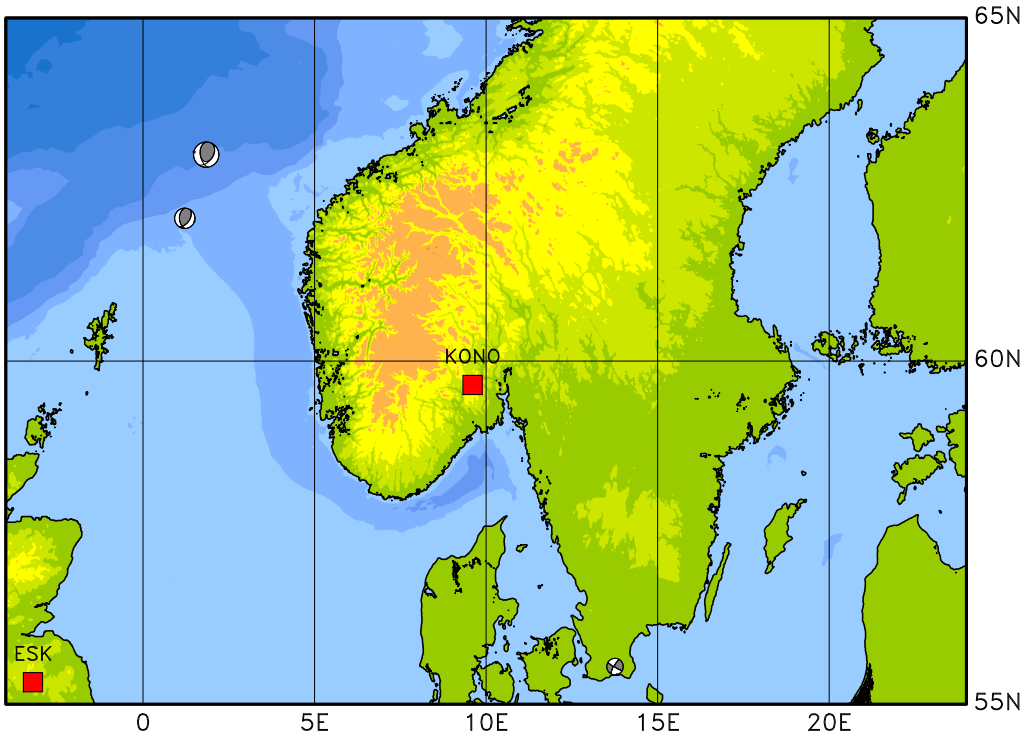

Figure 1: Map showing the location of KONO (red square) in southern Norway. Grey focal mechanisms show the locations and moment tensors of earthquakes in the Global CMT catalog. The closest GSN station is ESK-II, located ∼900 km to the southwest in Scotland.

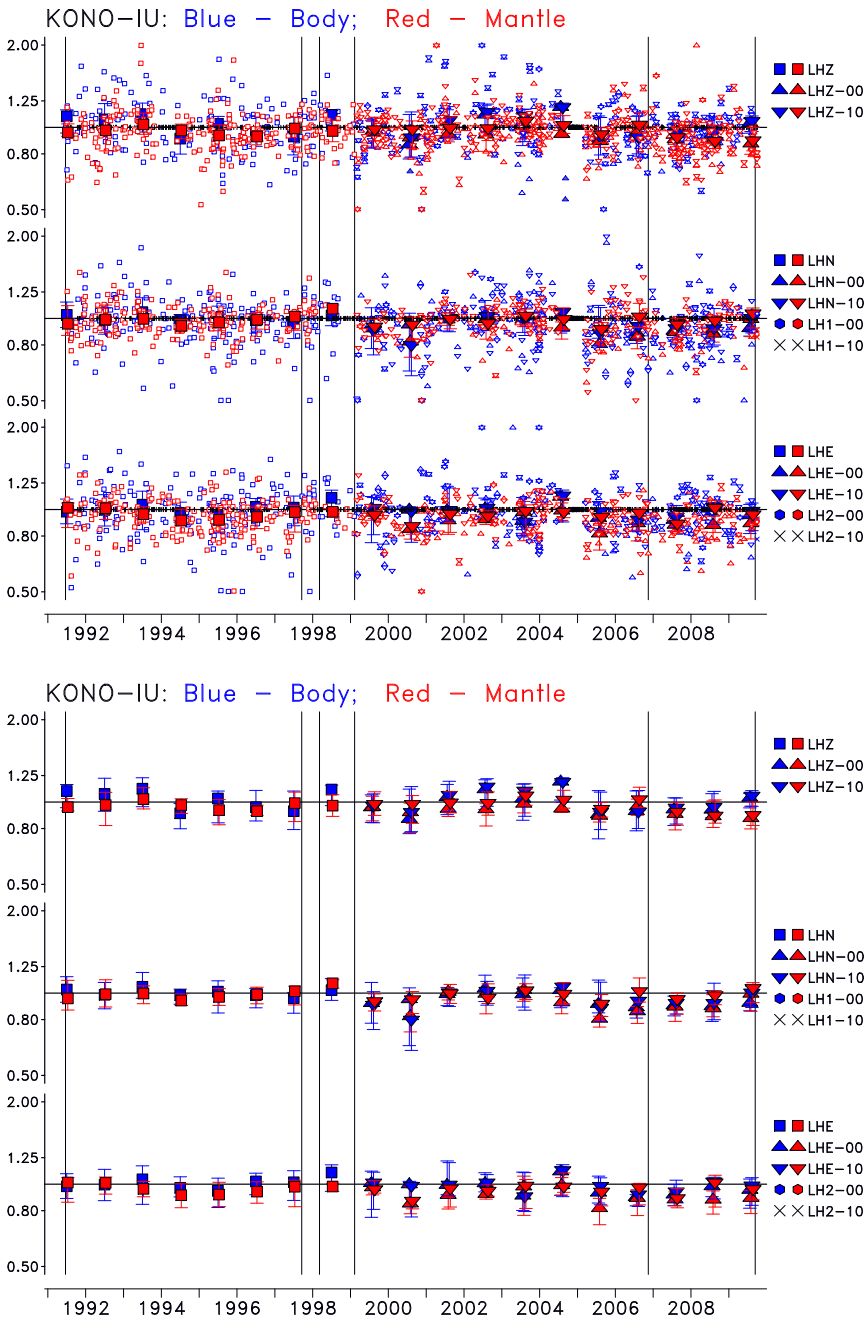

Figure 2: Scaling factors for the various data channels at KONO. Small symbols in top panel show scaling factors for individual traces. Tick marks on the horizontal axes show times of observations for which the correlation was less than 0.75. Large symbols show the median scaling factor for each year, with the error bars corresponding to the range of the second and third quartiles of the scaling factors. The legend on the right identifies the symbol type with a specific channel. Thin vertical lines show the response epoch boundaries present in the metadata. Bottom panel: same, but showing only the annual median values.

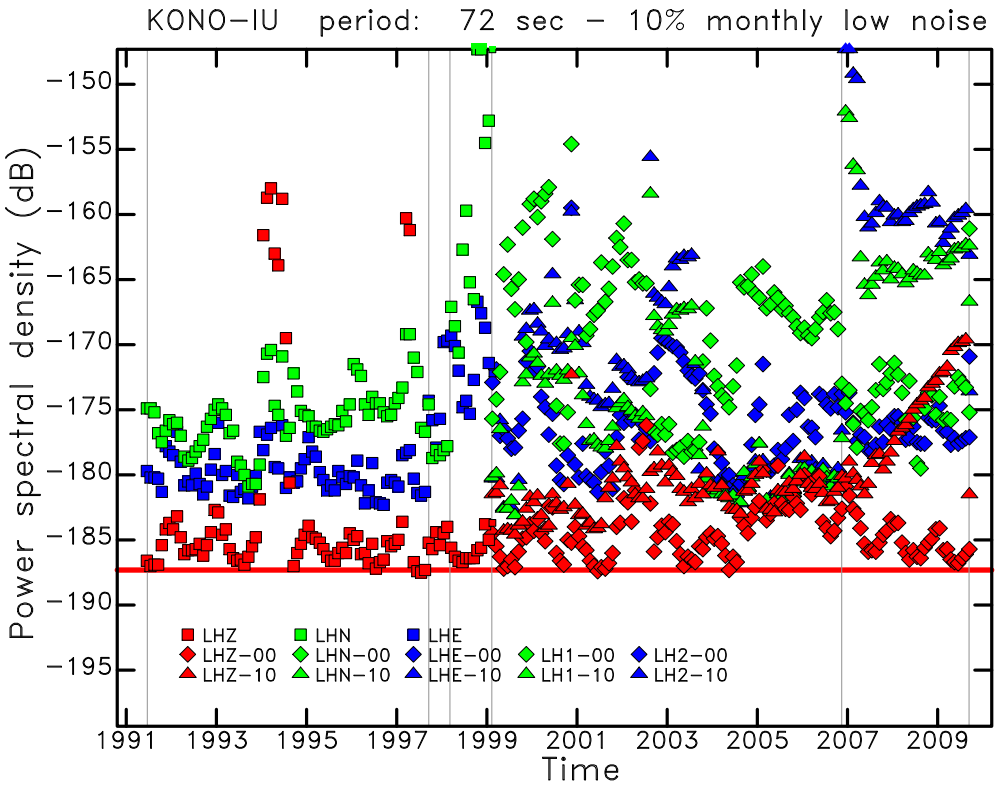

Figure 3: Monthly PSD of ground acceleration at 72-s period for all long-period (LH) channels at KONO for the period 1991–2009. Smaller symbols are used for months with fewer available hourly measurements. Each component and sensor is represented by a distinct symbol and color. The red horizontal line indicates the level of Peterson's (1993) Low Noise Model (LNM) at 72 s. The thin vertical lines show the times of epoch boundaries in the station metadata.

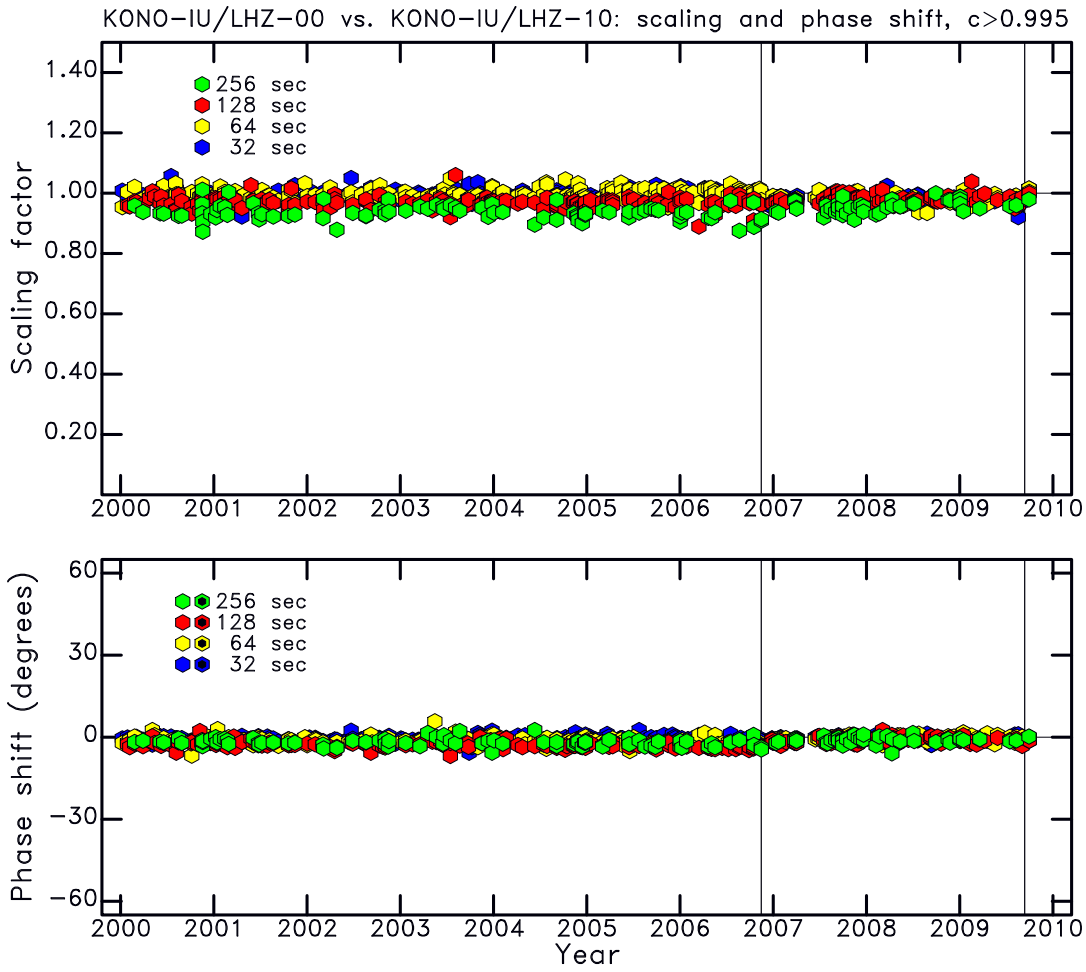

Figure 4: Diagram shows the result of coherence analysis for the vertical components of the STS-1 and STS-2 sensors. Each symbol represents a measurement of coherence for a $M_W \geq 6.5$ earthquake. The minimum coherence plotted is indicated by c. The scaling and phase shift between the two time series is shown at four different periods. The small deviations of the coherence measurements from a scaling of 1.0 and a phase shift of 0° show that the calibrations are generally consistent, though longer periods show evidence for slightly overstated gains in the STS-1 metadata. The thin vertical lines show the times of epoch boundaries in the station metadata.

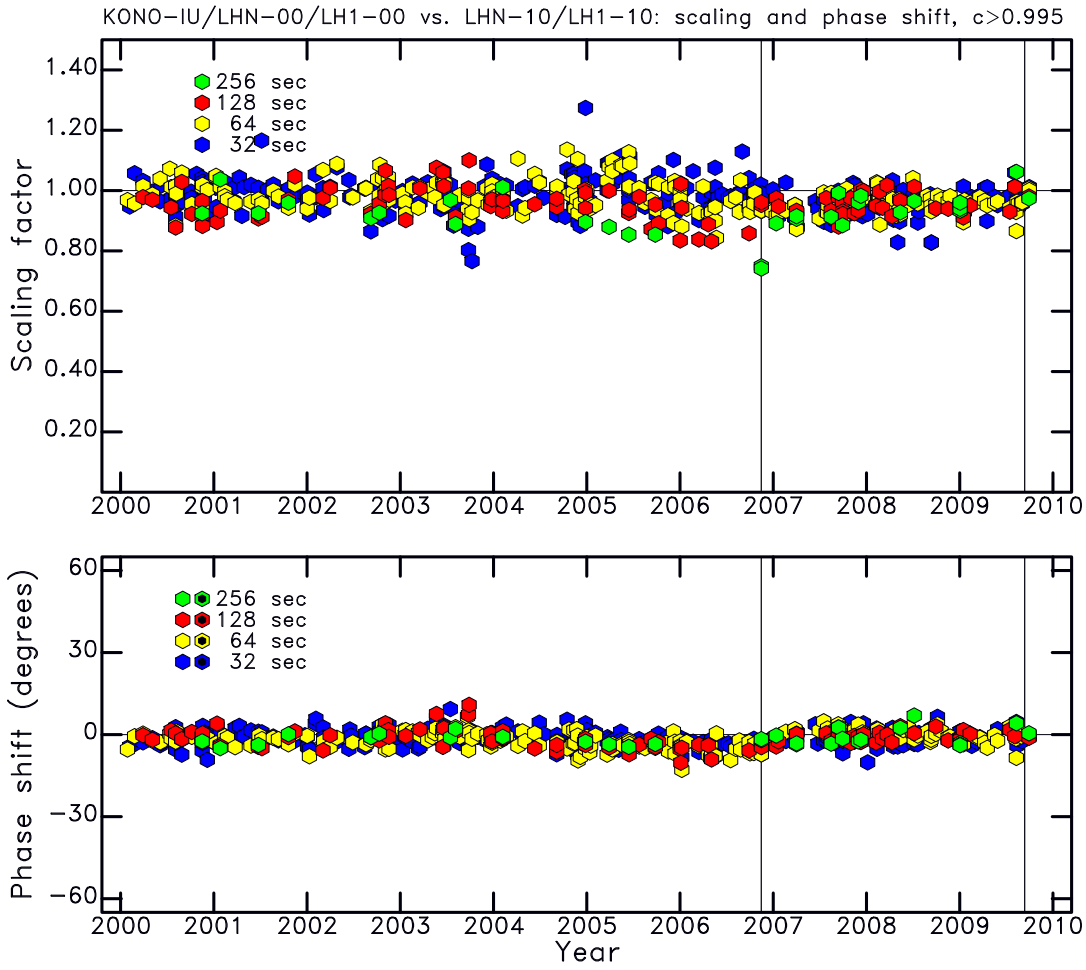

Figure 5: Same as Figure 4, but for the North-South components.

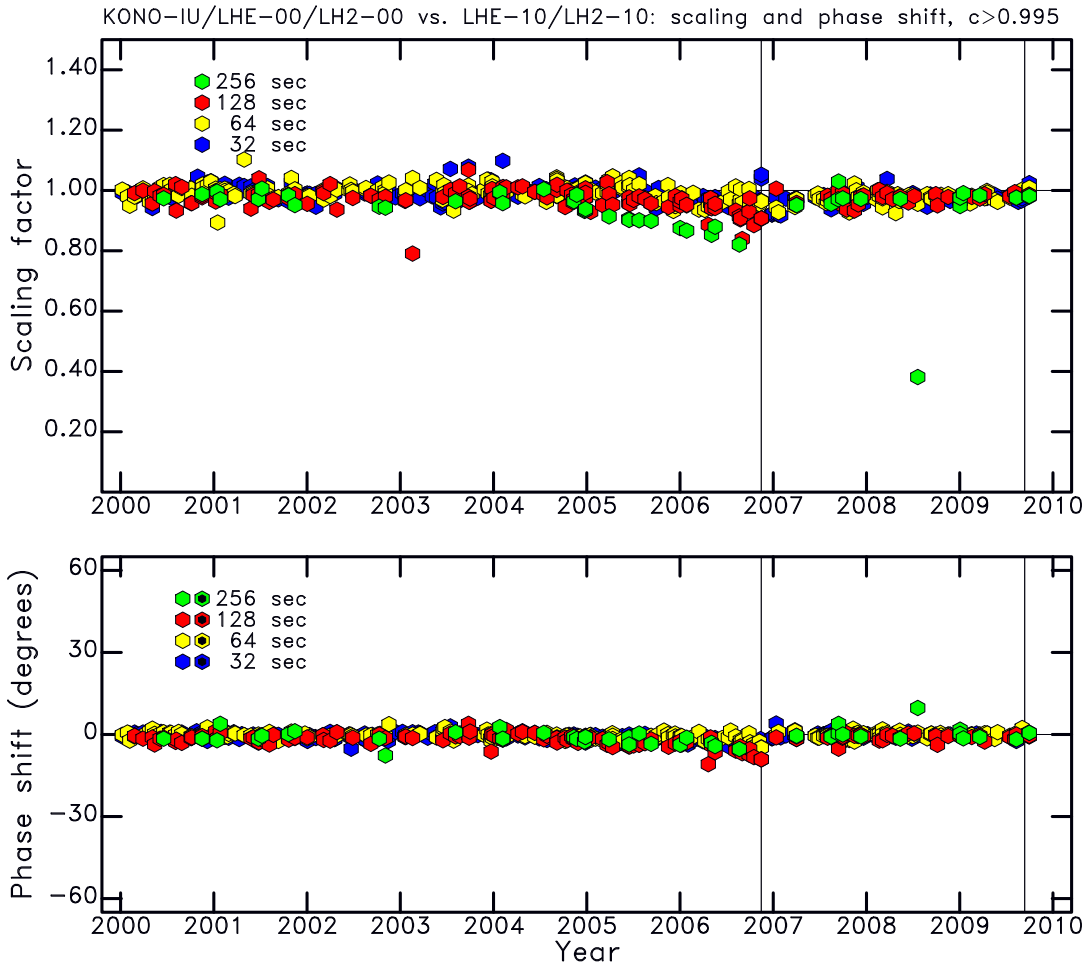

Figure 6: Same as Figure 4, but for the East-West components. A loss of long-period gain occurs between 2004 and late 2006.

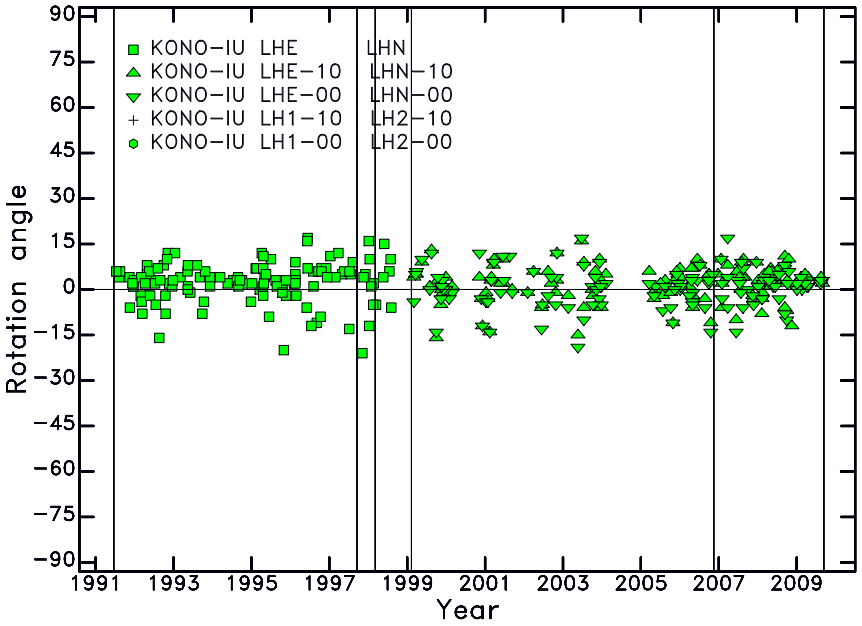

Figure 7: Individual measurements of polarization angle as a function of time. All measurements for the period of operation are shown. Symbols represent measurements obtained in the surface-wave band of the CMT analysis. More than 50% of the observations lie in the range -5° to $+1^\circ$ for the STS-1 sensor and in the range -3° to 3° for the STS-2 sensor. The thin vertical lines show the times of epoch boundaries in the station metadata.

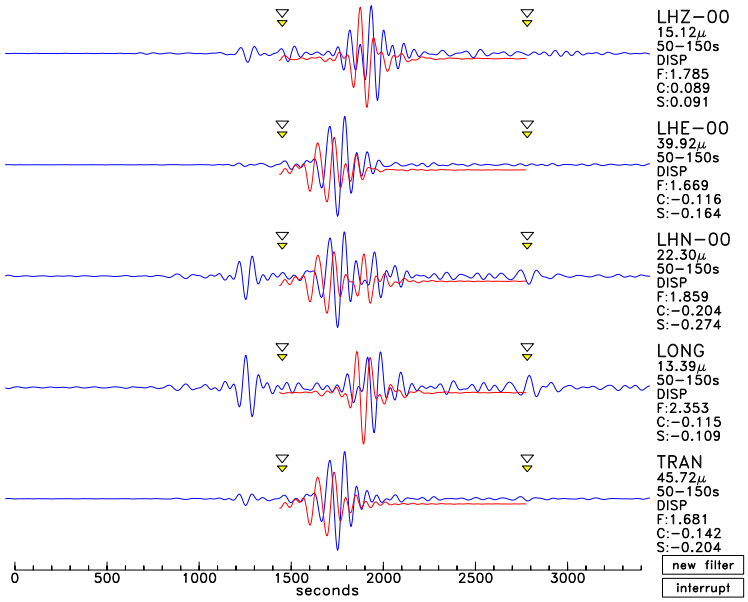

Figure 8: Observed and synthetic surface-wave seismograms for an earthquake on November 2, 2004. The synthetic waveforms are approximately 60 seconds early with respect to the observed seismograms. This is a reflection of a timing error that existed at the station for part of 2004 and 2005.

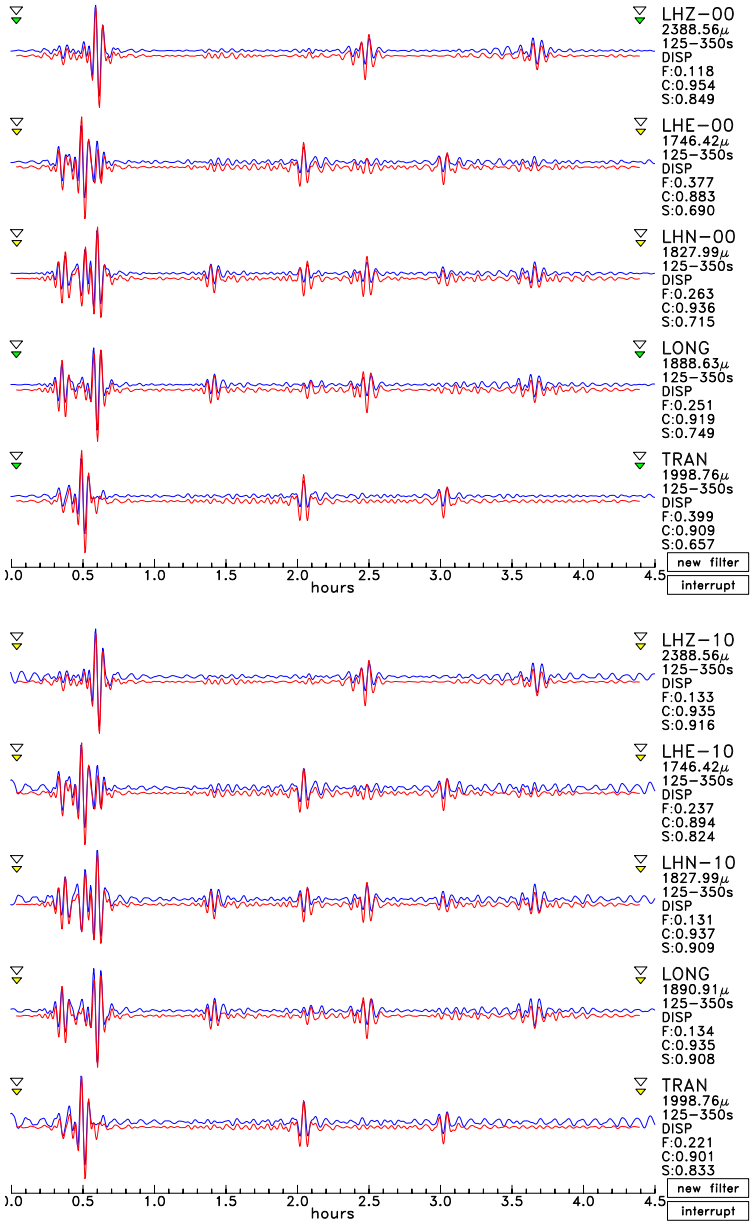

Figure 9: (Top) Observed (STS-1) and synthetic mantle-wave seismograms for an earthquake ($M = 8.3$) on November 15, 2006. The correlation between the two (C in right-hand column) is high, but scaling factors deviate significantly from 1.0. (Bottom) Observed (STS-2) and synthetic mantle-wave seismograms for the same earthquake, but recorded on the STS-2 seismometer. The fit to all three components is very good. Scaling factors are different from those of the STS-1 seismograms by 5–20% for the three components.

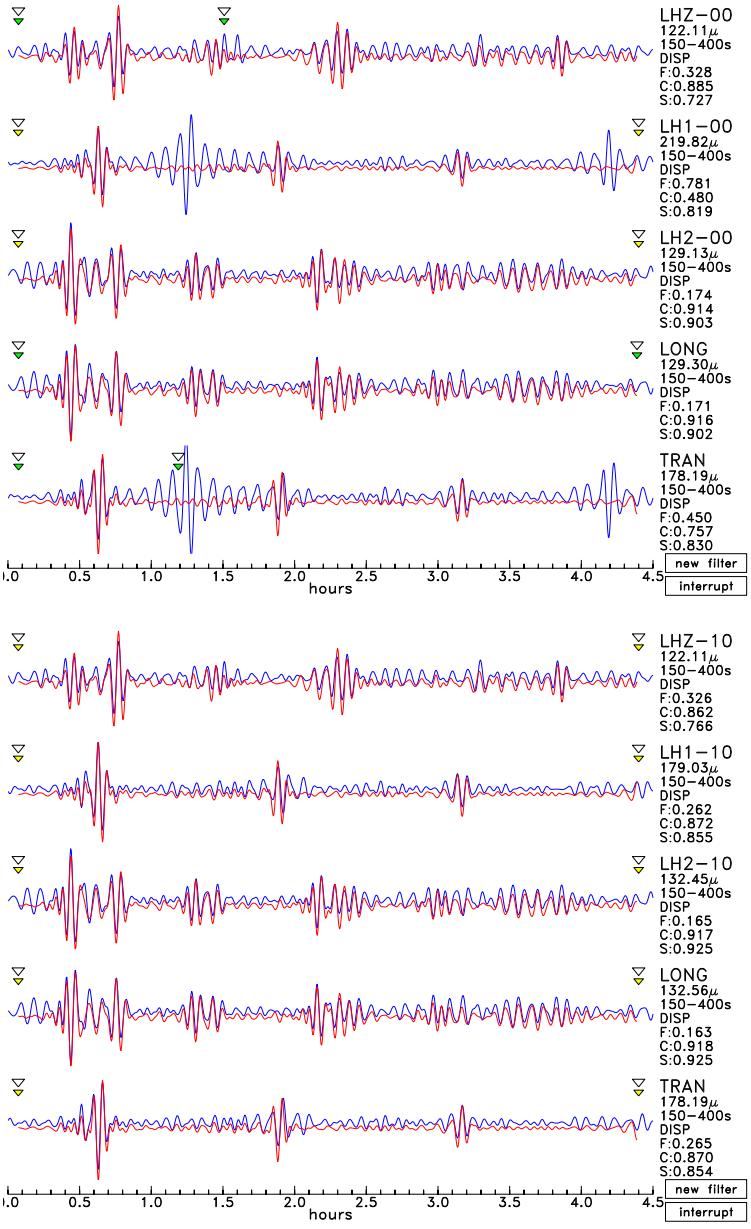

Figure 10: (Top) Observed (STS-1) and synthetic surface-wave seismograms for an $M = 7.6$ earthquake on September 30, 2009. The fit is good, apart from two noise pulses on the LH1-00 component. (Bottom) Observed (STS-2) and synthetic body-wave seismograms for the same earthquake, but recorded on the STS-2 seismometer. The LH1 noise pulses are not present on the STS-2 sensor. The scaling factors for the two sensors are similar.